Sensors & Transducers, Vol. 188, Issue 5, May 2015, pp. 33-39

Sensors & Transducers

http://www.sensorsportal.com

Electrochemical Detection of Hydrazine and 4-Nitrophenol Based on Layer-by-Layer Assembled Multilayer Films of Reduced Graphene Oxide/Gold Nanoparticles

[1] Shuohan HUANG, [2] Yueshan ZHOU, [1] Yan GAO, [1] Lei XU and [1] Huijun JIANG

[1] School of Pharmacy, Nanjing Medical University, No.140, Hanzhong Road, Nanjing 210029, PR China

[2] Nanjing Jinling Secondary Vocational School, Nanjing 210014, PR China

E-mail: huijun_jiang@njmu.edu.cn

Received: 5 April 2015 /Accepted: 5 May 2015 /Published: 29 May 2015

Abstract: Based on poly sodium 4-styrenesulfonate (PSS) functionalized reduced graphene oxide (RGO) and polyamidoamine (PAMAM) dendrimer protected gold nanoparticles (AuNPs), a novel electrochemical sensing platform for sensitive detection of 4-nitrophenol and hydrazine was fabricated via electrostatic layer-by-layer (LBL) self-assembly on a gold electrode modified with a first layer of poly (diallyldimethylammonium chloride) (PDDA). The resulting nanocomposites were characterized by Raman and UV-Vis spectroscopes. Besides, electrochemical measurements were employed to investigate the electrocatalytic and sensing properties of the as-prepared modified electrode. The results indicate that the LBL assembled PSS-RGO/PAMAM-AuNPs multilayer films possess excellent electrocatalytic activities towards the reduction of 4-nitrophenol (4-NP) and the oxidation of hydrazine and also show good analytical performance for the amperometric detection of the potential poisonous substances. In addition, the combination of the reduced graphene oxide and gold nanoparticles in the LBL assembly films and their synergistic effect may account for the increased electrochemical activities.

Keywords: Reduced graphene oxide, Layer-by-layer, Gold nanoparticle, Hydrazine, 4-Nitrophenol.

1. Introduction

Graphene, a two-dimensional carbon material with a single layer of carbon atoms packed densely in a honeycomb crystal lattice, has been considered as an excellent transducer material since its discovery in 2004 [1]. Due to its unique electrochemical and physical properties, graphene and graphene-based nanomaterials have shown great promise in a variety of applications, such as in light emitting diodes, touch screens, field-effect transistors, solar cells, supercapacitors, batteries, and sensors [2]. Several methods have been established to synthesize graphene, including mechanical/chemical exfoliation of graphite, opening/unzipping of carbon nanotubes (CNTs), chemical vapor deposition (CVD), epitaxial growth on electrically insulating surface, reduction of graphene oxide (GO) and many other synthetic methods. Oxidative exfoliation of pristine graphite is the most used method in the synthesis of graphene utilized in electrochemistry to get the aqueous dispersion of graphene oxide, followed by the chemical reduction to eliminate most oxygen functional groups [3]. Nevertheless, the chemical

reduced graphene oxide nanosheets tend to form irreversible agglomerates or restack via van der Waals interaction in the process of reduction and could not be re-dispersed in water by ultrasonication. As a result of that, the most common approaches to obtain stable graphene dispersions in water focus on the preparation of graphene materials either by covalent or noncovalent modifications to improve their properties or functions [4].

Polyamidoamine (PAMAM) dendrimers are monodispersed well-defined highly branched molecular (nano) architectures with tertiary amines in core, primary amines on the surface and an amide backbone [5]. They have attracted considerable attention in a variety of scientific fields, especially in chemical sensors and biosensors owing to their unique properties. Dendrimers with high generation numbers ($G \geq 4$) usually possess a nearly spherical shape and can encapsulate metal complexes, nanoparticles and other guest molecules. Different noble metal nanoparticles have been successfully synthesized at the surface of the dendrimers or encapsulated inside the dendrimers to form stable aqueous colloidal dispersions, such as Ag, Au, Pd and Pt nanoparticles [6]. Among these dendrimer-stabilized metal nanoparticles, gold nanoparticles (AuNPs) have been the most extensively studied metal material in the fabrication of electrochemical sensors due to their unique electrochemical properties, excellent biological components, ease of further modification and other related properties.

Self-assembly, especially layer-by-layer self-assembly (LBL) is a fundamental issue in the fields of nanotechnologies and nanomaterials, based on the rational assembly of a wide range of different building blocks raging from the atomic to the macroscopic levels [7]. The interactions between the building blocks may include hydrogen bonding, electrostatic attraction, π-π staking, donor-acceptors, van der Waals, hydrophilic or hydrophobic interactions, and a number of others [8]. At the present, it is still an effective way for the fabrication of electrochemical sensors for its accurate control of film thickness, structures and building blocks.

4-Nitrophenol (4-NP), an aromatic phenolic compound widely used in the manufacturing of the most popular analgesics, pesticides, dyes, and in processing of leather, can be inevitably released to the environment [9]. Moreover, acute inhalation or ingestion of 4-NP in a short time can cause headaches, drowsiness, nausea, cyanosis and it was even reported as a potential carcinogen, teratogen and mutagen. US Environmental Protection Agency (EPA) has considered it as a hazardous waste and high-priority toxic pollutant [10]. Therefore simple and reliable method for the determination of 4-nitrophenol is of prime importance.

Hydrazine, a colorless liquid compound, has received increased attention recently due to its various applications in many fields. However, hydrazine and its derivatives are commonly known as neurotoxin and have been reported to have adverse health effects to human organs, such as lungs, livers, kidneys, respiratory tracts, and central nervous systems [11]. Various methods including colorimetric method, chemiluminescence method, flow injection and so on have been used to detect hydrazine. Recently, electrochemical detection of hydrazine has been emerged due to its high sensitivity and low cost.

Herein, poly sodium 4-styrenesulfonate (PSS) functionalized reduced graphene oxide and dendrimer-encapsulated gold nanoparticles were used as the building blocks to fabricate a multilayer film on the gold electrode via electrostatic LBL self-assemble technique. The prepared nanocomposites were characterized by Raman spectroscopy and ultraviolet visible (UV-Vis) absorption spectroscopy. In addition, the electrocatalytic activities towards 4-nitrophenol and hydrazine and the potential sensing performance are evaluated.

2. Experimental

2.1. Reagents and Chemicals

Graphite powder (Alfa Aesar., 99.9995 %), Poly (sodium 4-styrenesulfonate) (Sigma-Aldrich), amino-terminated PAMAM dendrimer (Sigma-Aldrich, generation 4, 10 wt % in methanol) were used as received. Poly (diallyldimethylammonium chloride) was purchased from Nittobo Co. as an aqueous solution. 4-nitrophenol, chloroauric acid, and hydrazine solution (85 wt %) were all purchased from Shanghai Chemical Reagent Co. Ltd. Other chemicals used were of analytical grade. All aqueous solutions were prepared using ultrapure water. The phosphate buffer solution (PBS) was prepared by mixing the 0.1 M Na_2HPO4-NaH_2PO4.

2.2. Synthesis of PSS-functionalized Reduced Graphene Oxide

The exfoliated GO was synthesized from graphite powder by a modified Hummers method [12]. The obtained homogeneous GO dispersion (60 mg) was mixed with 600 mg PSS by ultrasonication for 30 min, and then stirred at 50 °C for 24 h. After cooling, 4 mL ammonia solution and 4 mL hydrazine solution were added, the mixture was kept at 95 to 100 °C for 24 h. The dispersion was then centrifuged and redispersed in water by ultrasonication to obtain PSS-functionalized reduced graphene oxide (PSS-RGO).

2.3. Preparation of PAMAM Protected AuNPs

PAMAM protected AuNPs were prepared as follows: 4.8 mL $HAuCl_4$ solution (1.4 mM) was incrementally added (with at least 30 min between

additions) to 1.0 mL PAMAM (0.1 mM) and 10.5 mL water with stirring in darkness for 24 h. Then, 7.0 mL formic acid (0.1 mM) was gradually added and the mixed solution was stirred vigorously for another 24 h to ensure the completion of the reaction and aggregation process.

2.4. Fabrication of [PSS-RGO/PAMAM-AuNPs]$_n$ Multilayer Films

A freshly cleaned gold electrode was dipped in positively charged PDDA solution (1.0 wt %) for 30 min to form a monolayer of PDDA. Then the modified electrode was rinsed with water to clean the weakly absorbed molecules. The fabrication process of Layer-by-layer self-assembly of PSS-functionalized reduced graphene oxide and PAMAM protected AuNPs composite is illustrated in Fig. 1. The fabrication involved three stages: (A) The modified gold electrode with positive surface charges was immersed in a negatively charged solution of RGO for 20 min. (B) Then rinsing thoroughly with water before the electrode was treated with the positively charged solution of AuNPs for 20 min. (C) Further rinsing was performed to remove unabsorbed materials. The resulting film was defined as one bilayer. By repeating the assembly procedures (A), (B) and (C), the desired number of multi-layers was achieved.

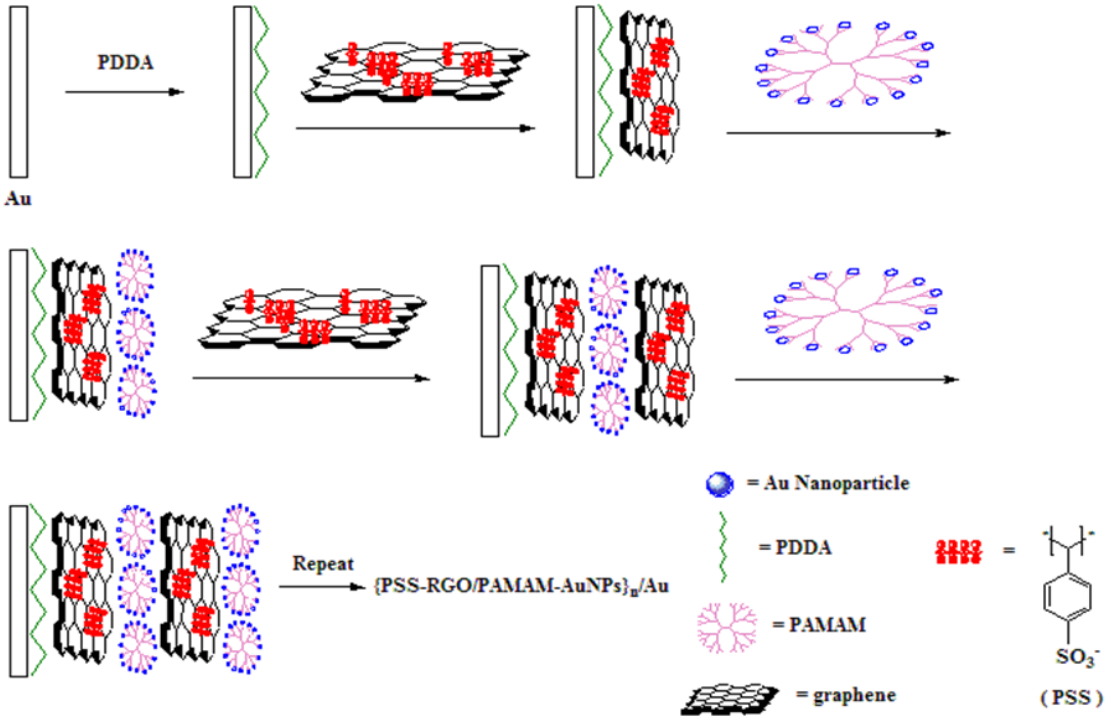

Fig. 1. Schematic illustration for the LBL self-assembly of [PSS-RGO/PAMAM- Au NPs]$_n$ multilayer films.

2.5. Instruments

The electrochemical measurements were obtained by using a CHI 760C Potentiostat (Shanghai Chenhua Co., China). A three-electrode system consisting of a gold electrode as working electrode, a platinum wire and a saturated calomel electrode (SCE) as the counter electrode and reference electrode respectively was employed for all the potential values reported. High-purity nitrogen was used for the deaeration of the solutions. During the measurements, a gentle nitrogen flow was kept above the electrolyte surface. All electrochemical experiments were performed at 25 ± 1 °C.

UV–Vis absorption spectra were obtained using a Perkin-Elmer Lambda 18 spectrophotometer over the spectral range 200-800 nm. Raman spectra were measured on an HR800 Horiba Jobin Yvon Raman Microprobe with a laser wavelength of 632.8 nm.

3. Results and Discussion

3.1. Characterization of PSS-functionalized Reduced Graphene Oxide and PAMAM Protected Gold Nanoparticles

The Raman spectra of graphene oxide, graphene nanosheets and PSS-RGO are shown in Fig. 2. The Raman spectrum of the graphene oxide (curve a) displays two characteristic peaks: the well-recognized D band at 1328 cm^{-1} and the G band at 1592 cm^{-1}.

When GO was chemically reduced, the D band and G band shifted to 1329 cm^{-1} and 1587 cm^{-1} (curve b), respectively, with an increase in the intensity ratio of I_D/I_G (1.52) compared to that of GO (1.36). These observations further confirm the graphitization in reduced graphene nanoparticles [13]. In addition, after GO was functionalized with PSS and reduced by hydrazine hydrate, no obvious shifts were observed (curve c), indicating that the structure of the graphene nanosheets did not change after the fabrication of PSS on the surface of RGO.

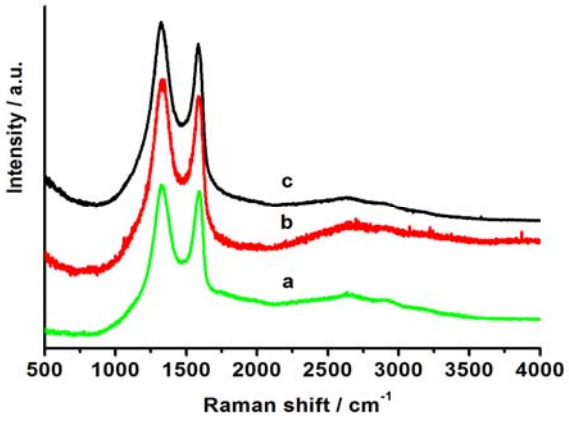

Fig. 2. Raman spectra of (a) graphene oxide; (b) graphene nanosheets and (c) PSS-RGO excited at 632.8 nm wavelength.

UV-Vis spectroscopy was employed to investigate the formation of the Au nanoparticles protected by PAMAM (Fig. 3).

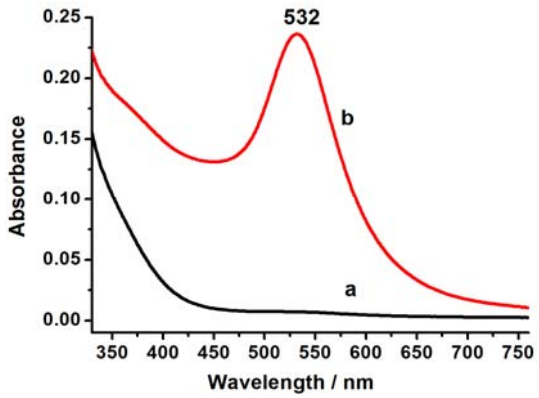

Fig. 3. UV-Vis spectra of PAMAM dendrimer-$HAuCl_4$ aqueous solution before (a) and after (b) reduction with formic acid.

After the reduction with formic acid, the change of solution color (from light yellow to mauve) suggests the reduction of Au^{3+} to Au^0. In addition, obvious surface plasmon resonance absorption was observed at 523 nm after the reduction, revealing the successful formation of colloidal gold nanoparticles protected by PAMAM dendrimer [14].

3.2. Electrochemical Characterization of Layer-by-layer Assembled Multilayer Films

The cyclic voltammograms of 5 mM $K_3[Fe(CN)_6]$ in 0.1 M KCl was performed at the modified electrode at different scan rates range from 10 to 100 mV/s (Fig. 4). With the increase of the scan rates, the anodic peak potential shifts positively and the cathodic peak potential shifts negatively, indicating that redox reaction becomes irreversible. Moreover, the anodic peak current was proportional to the square root of the scan rate (inset in Fig. 4), and the equation was I (μA) = 2.602 $v^{1/2}$ + 1.328 (r = 0.998). These results demonstrated that the redox process of $K_3[Fe(CN)_6]$ on the modified electrode was a typical diffusion controlled electrochemical process.

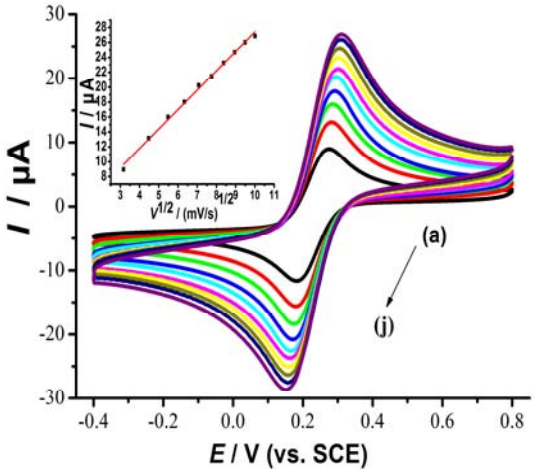

Fig. 4. CVs of the [PSS-RGO/PAMAM-AuNPs]$_{20}$/AuE in 5 mM $K_3[Fe(CN)_6]$ in 0.1 M KCl solution at scan rates of 10, 20, 30, 40, 50, 60, 70, 80, 90 and 100 mV/s (from a to j). *Insert:* linear relationship between the anodic peak current and the square root of the scan rate.

3.3. Electrochemical Behavior of 4-Nitrophenol at the Modified Electrode

To improve the sensitivity of the 4-NP determination, the prepared sensor was accumulated in the solution for an accumulation time of 180 s at an accumulation potential of 0.0 V before each experiment. Fig. 5 shows the typical CVs of the modified electrode in 0.1 M phosphate buffer solution (PBS) (pH 6.0) with the different concentrations of 4-NP. A well-defined cathodic peak corresponding to the electrochemical reduction of 4-NP was observed at – 0.668 V. Moreover, the reduction current increased with the increase in 4-NP concentration, implying that the PSS-RGO/PAMAM-AuNPs multilayer films can effectively catalyze the electrochemical reduction of 4-NP.

The effect of solution pH on the voltammetry was examined by CVs in the pH range of 5.0-9.0 (Fig. 6A). As shown in Fig. 6B, the cathodic

reduction peak potential shifted linearly to the negative direction with the increasing pH values. The maximum peak current was obtained at pH 6.0 (Fig. 6C). Thus PBS (pH 6.0) was chosen in the following analytical experiments.

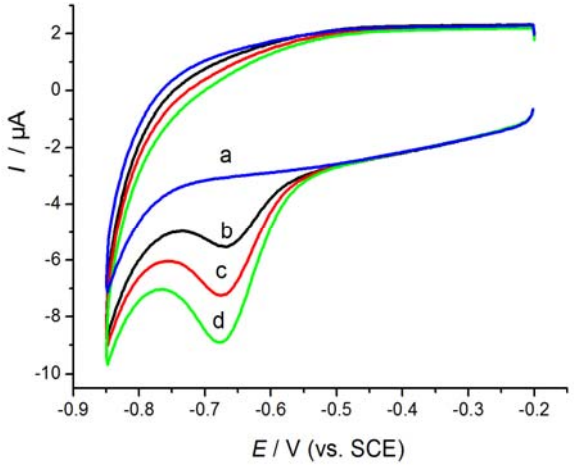

Fig. 5. CVs of $[PSS\text{-}RGO/PAMAM\text{-}AuNPs]_{20}$/AuE in 0.1 M phosphate buffer solution (pH 6.0) at scan rate of 100 mV/s in the presence of (a) 0, (b) 0.2, (c) 0.4, and (d) 0.6 μM 4-nitrophenol.

To evaluate the application of the modified electrode for the detection of 4-NP, amperometric response was monitored by successively injection of 4-NP into the PBS under optimized conditions (pH 6.0) at an applied potential of 0.65 V (shown in Fig. 7). The electrocatalytic current was linearly dependent on the concentration of 4-nitrophenol within the range from 5 to 515 μmol L^{-1} with a detection limit of 1.8 μmol L^{-1} based on the signal-to noise ratio of 3 (insert in Fig. 7). The comparison between previously reported modified electrodes for 4-NP detection is listed in Table 1. It can be seen that $[PSS\text{-}RGO/PAMAM\text{-}AuNPs]_{20}$/AuE exhibited a relatively wide linear range.

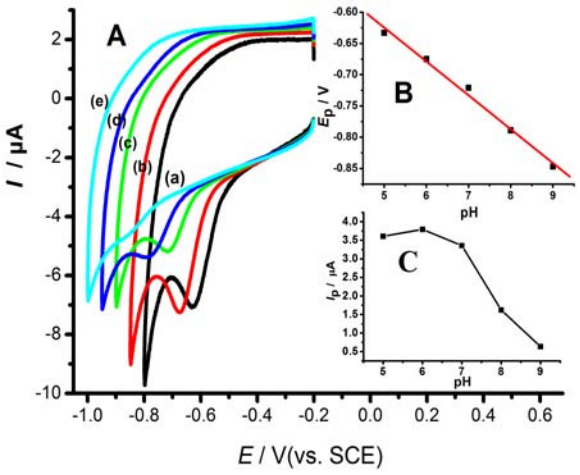

Fig. 6. (A) CVs of $[PSS\text{-}RGO/PAMAM\text{-}AuNPs]_{20}$/AuE at a scan rate of 100 mV/s in PBS with different pH values (a) 5.0, (b) 6.0, (c) 7.0. (d) 8.0, (e) 9.0 of 0.4 μM 4-nitrophenol; (B) Effects of the pH value on the cathodic reduction peak potentials; (C) Effects of the pH value on the peak current.

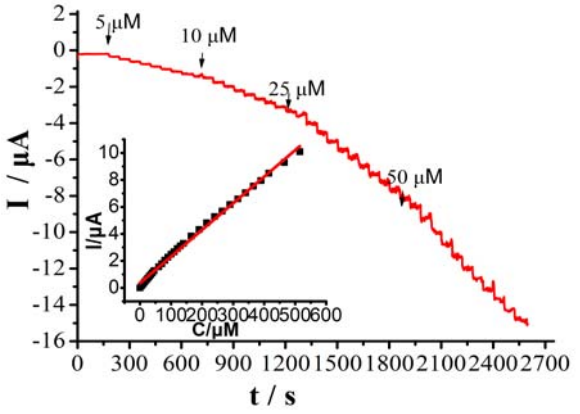

Fig. 7. Typical amperometric response of the $[PSS\text{-}RGO/PAMAM\text{-}AuNPs]_{20}$/AuE at ‐ 0.65 V on successive injection of 4-nitrophenol into 2 mL of stirring 0.1 mol/L PBS (pH 6.0). *Insert*: linear relationship between reduction current on the concentration.

Table 1. Comparison of different modified electrodes for the determination of 4-NP.

Electrode materials	Detection limit(μM)	Linear range(μM)	References
GO/GCE	0.02	0.1-120	[15]
BDD-MEA	0.22	1.8-9.2	[16]
AgSA-PE	1.0	1-100	[10]
AaP/AuNPs	0.2	10-30	[17]
PB modified electrodes	8.23	30-90	[18]
$[PSS\text{-}RGO/PAMAM\text{-}AuNPs]_{20}$	1.8	5-515	This work

3.4. Electrochemical Behavior of Hydrazine at the Modified Electrode

Fig. 8 illustrates the typical CVs of a bare gold electrode (curve a, c) and $[PSS\text{-}RGO/PAMAM\text{-}AuNPs]_{20}$/AuE (curve b, d) in an N_2-saturated PBS solution (pH 7.4) at a scan rate of 100 mV/s in the presence of 0 (curve a, b) and 0.4 mM hydrazine (curve c, d). It demonstrates clearly that both bare gold electrode and [PSS-RGO/PAMAM-

AuNPs]$_{20}$/AuE exhibits no electrochemical response in the absence of hydrazine. However, a well-defined oxidation peak was observed at bare gold electrode at 0.465 V in response to the anodic oxidation of hydrazine. In addition, there exhibited an enhanced increase of the electrocatalytic current with the oxidation peak located at 0.357 V in the presence of hydrazine at the [PSS-RGO/PAMAM-AuNPs]$_{20}$/AuE. These results indicated that the nanocomposites could significant promote the electrocatalytic activity toward the oxidation of hydrazine.

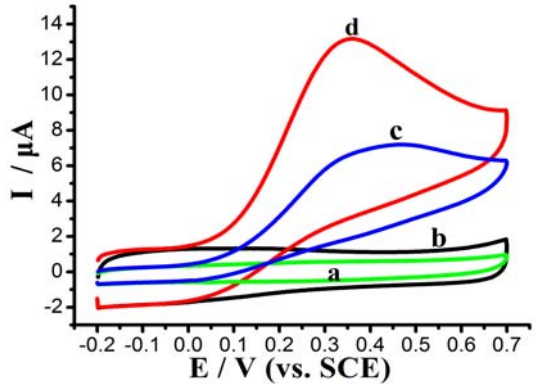

Fig. 8. CVs of the bare gold (a, c) and [PSS-RGO/PAMAM-AuNPs]$_{20}$/AuE (b, d) in a buffer solution (pH 7.4) at a scan rate of 100 mV/s in the presence of 0 (a, b), 0.4 mM hydrazine (c, d).

Fig. 9 shows the amperometric response of the [PSS-RGO/PAMAM-AuNPs]$_{20}$/AuE modified electrode in 2.0 mL of stirring 0.1 mol/L buffer solution (pH 7.4) on continuous step change of hydrazine concentration at an optimized potential at 0.35 V. As illustrated, upon each addition of hydrazine, the sensor showed fast response and accomplished a steady-state current with the average response time of 2 s. The catalytic current increased linearly with the increasing concentration of hydrazine ranging from 5 μM to 900 μM with the linear regression equation as I (μA) = = 0.01256C (μM) + 0.4136 (r = 0.998). The detection limit is estimated to be 0.24 μM (S/N = 3). To evaluate the sensing performance of [PSS-RGO/PAMAM-AuNPs]$_{20}$/AuE, the comparison was shown in Table 2 with those reported previously in the literatures. As can be seen, the detection limit of this work is lower in comparison with other modified electrodes with a relatively wide range of hydrazine.

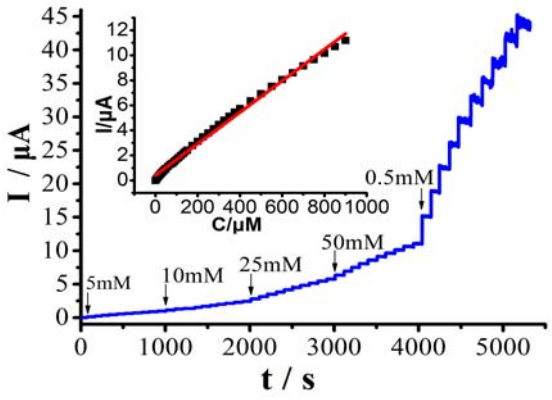

Fig. 9. Typical amperometric response of the [PSS-RGO/PAMAM-AuNPs]$_{20}$/AuE at 0.35 V on successive injection of hydrazine into 2.0 mL of stirring 0.1 mol/L buffer solution (pH 7.4). *Insert*: linear relationship between the current and concentration.

Table 2. Comparison of different modified electrodes for the determination of hydrazine.

Electrode materials	Detection limit(μM)	Linear range(μM)	References
Graphene	1.0	3.0-300	[19]
Co-salen/SWNHs	0.96	1-96	[20]
AuNP-GPE	3.07	25-1000	[21]
Pd/MWNT-Nafion modified electrode	1.0	2.5-700	[22]
Nano-Au/Porous-TiO_2	0.5	2.5-500	[23]
CuS/rGO	0.3	1-1000	[24]
[PSS-RGO/PAMAM-AuNPs]$_{20}$	0.24	5-900	This work

4. Conclusions

In this work, an electrochemical sensor based on layer-by-layer self-assembly of PAMAM dendrimer protected gold nanoparticles and PSS functionalized reduced graphene oxide by using the electrostatic layer-by-layer self-assembly technique was fabricated. The combination and synergistic effect of gold nanoparticles and reduced graphene oxide hold the promise for the enhanced electrocatalytic performance towards the reduction of 4-nitrophenol and the oxidation of hydrazine. Moreover, the electrochemical sensor was applied for the detections of trace 4-nitrophenol and hydrazine, and exhibited favorable sensing performance. Therefore, these novel nanocomposites have great potential and could be used to fabricate sensitive sensors in environment, medicine and biotechnology.

Acknowledgements

This work was supported by Natural Science Foundation of Jiangsu Province (No.BK2014143).

References

[1]. J. Yu, L. Yu, H. Yang, Q. Liu, X. Chen, X. Jiang, X. Chen, and F. Jiao, Graphene nanosheets as novel adsorbents in adsorption, preconcentration and removal of gases, organic compounds and metal ions, *Science of The Total Environment*, Vol. 502, Issue 70, 2015, pp. 70-79.

[2]. A. T. Lawal, Synthesis and utilisation of graphene for fabrication of electrochemical sensors, *Talanta*, Vol. 131, Issue 424, 2015, pp. 424-443.

[3]. K. R. Ratinac, W. Yang, J. J. Gooding, P. Thordarson, and F. Braet, Graphene and Related Materials in Electrochemical Sensing, *Electroanalysis*, Vol. 23, Issue 4, 2011, pp. 803-826.

[4]. C. Li, and G. Shi, Synthesis and electrochemical applications of the composites of conducting polymers and chemically converted graphene, *Electrochimica Acta*, Vol. 56, Issue 28, 2011, pp. 10737-10743.

[5]. F. Zhao, and W. Li, Dendronized graphenes: remarkable dendrimer size effect on solvent dispersity and bulk electrical conductivity, *Journal of Materials Chemistry*, Vol. 22, Issue 7, 2012, pp. 3082-3087.

[6]. B. Kavosi, A. Salimi, R. Hallaj, and K. Amani, A highly sensitive prostate-specific antigen immunosensor based on gold nanoparticles/PAMAM dendrimer loaded on MWCNTS/chitosan/ionic liquid nanocomposite, *Biosensors and Bioelectronics*, Vol. 52, Issue 15, 2014, pp. 20-28.

[7]. M, M. A. S. A, Self-assembly from milli- to nanoscales: methods and applications, *Journal of Micromechanics and Microengineering*, Vol. 19, Issue 8, 2009, pp. 083001-083038.

[8]. X. C. Jiang, Q. H. Zeng, C. Y. Chen, and A. B. Yu, Self-assembly of particles: some thoughts and comments, *Journal of Materials Chemistry*, Vol. 21, Issue 42, 2011, pp. 16797-16805.

[9]. X. X. Jiao, H. Q. Luo, and N. B. Li, Fabrication of graphene–gold nanocomposites by electrochemical co-reduction and their electrocatalytic activity toward 4-nitrophenol oxidation, *Journal of Electroanalytical Chemistry*, Vol. 691, 2013, pp. 83-89.

[10]. A. Danhel, B. Yosypchuk, V. Vyskocil, J. Zima, and J. Barek, A novel paste electrode based on a silver solid amalgam and an organic pasting liquid, *Journal of Electroanalytical Chemistry*, Vol. 656, Issue 1–2, 2011, pp. 218-222.

[11]. R. Devasenathipathy, V. Mani, and S. Chen, Highly selective amperometric sensor for the trace level detection of hydrazine at bismuth nanoparticles decorated graphene nanosheets modified electrode, *Talanta*, Vol. 124, 2014, pp. 43-51.

[12]. W. He, H. Jiang, Y. Zhou, S. Yang, X. Xue, Z. Zhou, D. L. Akins, and H. Yang, An efficient reduction route for the production of Pd–Pt nanoparticles anchored on graphene nanosheets for use as durable oxygen reduction electrocatalysts, *Carbon*, Vol. 50, Issue 1, 2012, pp. 265-274.

[13]. X. Dong, Q. Long, J. Wang, M. B. Chan-Park, Y. Huang, W. Huang, and P. Chen, A graphene nanoribbon network and its biosensing application, *Nanoscale*, Vol. 3, 2011, pp. 5156-5160.

[14]. J. Zhu, L. Zheng, S. Wen, Y. Tang, M. Shen, G. Zhang, and X. Shi, Targeted cancer theranostics using alpha-tocopheryl succinate-conjugated multifunctional dendrimer-entrapped gold nanoparticles, *Biomaterials*, Vol. 35, Issue 2, 2014, pp. 7635-7646.

[15]. J. Li, D. Kuang, Y. Feng, F. Zhang, Z. Xu, and M. Liu, A graphene oxide-based electrochemical sensor for sensitive determination of 4-nitrophenol, *Journal of Hazardous Materials*, Vol. 201–202, 2012, pp. 250-259.

[16]. N. S. Lawrence, M. Pagels, A. Meredith, T. G. J. Jones, C. E. Hall, C. S. J. Pickles, H. P. Godfried, C. E. Banks, R. G.compton, and L. Jiang, Electroanalytical applications of boron-doped diamond microelectrode arrays, *Talanta*, Vol. 69, Issue 4, 2006, pp. 829-834.

[17]. L. Peng, U. Wollenberger, M. Hofrichter, R. Ullrich, K. Scheibner, and F. W. Scheller, Bioelectrocatalytic properties of Agrocybe aegerita peroxygenase, *Electrochimica Acta*, Vol. 55, Issue 27, 2010, pp. 7809-7813.

[18]. S. Lupu, C. Lete, M. Marin, N. Totir, and P. C. Balaure, Electrochemical sensors based on platinum electrodes modified with hybrid inorganic–organic coatings for determination of 4-nitrophenol and dopamine, *Electrochimica Acta*, Vol. 54, Issue 7, 2009, pp. 1932-1938.

[19]. C. Wang, L. Zhang, Z. Guo, J. Xu, H. Wang, K. Zhai, and X. Zhuo, A novel hydrazine electrochemical sensor based on the high specific surface area graphene, *Microchim. Acta*, Vol. 169, Issue 1, 2010, pp. 1-6.

[20]. B. Lu, Z. Zhang, J. Hao, G. Xu, B. Zhang, and J. Tang, Electrochemical sensing platform based on Schiff-base cobalt(ii)/single-walled carbon nanohorns complexes system, *Analytical Methods*, Vol. 4, Issue 11, 2012, pp. 3580-3585.

[21]. M. Abdul Aziz, and A. Kawde, Gold nanoparticle-modified graphite pencil electrode for the high-sensitivity detection of hydrazine, *Talanta*, Vol. 115, 2013, pp. 214-221.

[22]. J. Zhao, M. Zhu, M. Zheng, Y. Tang, Y. Chen, and T. Lu, Electrocatalytic oxidation and detection of hydrazine at carbon nanotube-supported palladium nanoparticles in strong acidic solution conditions, *Electrochimica Acta*, Vol. 56, Issue 13, 2011, pp. 4930-4936.

[23]. G. Wang, C. Zhang, X. He, Z. Li, X. Zhang, L. Wang and B. Fang, Detection of hydrazine based on Nano-Au deposited on Porous-TiO2 film, *Electrochimica Acta*, Vol. 55, Issue 24, 2010, pp. 7204-7210.

[24]. Y. J. Yang, W. Li, and X. Wu, Copper sulfide|reduced graphene oxide nanocomposite for detection of hydrazine and hydrogen peroxide at low potential in neutral medium, *Electrochimica Acta*, Vol. 123, 2014, pp. 260-267.